International Journal of Steel Structures
https://doi.org/10.1007/s13296-018-0044-8

Seismic Performance Evaluation of Steel Diagrid Buildings

Joonho Lee[1] · **Jieun Kong**[1] · **Jinkoo Kim**[1]

Received: 7 January 2017 / Accepted: 20 February 2018

Abstract
In this study the seismic performances of axi-symmetric steel building structures with circular plan shape were evaluated based on the ATC-63 approach. For analysis models, thirty-three-story vertically convex, concave, and gourd-type axi-symmetric buildings were designed using diagrid structure system, and their seismic performances were compared with those of the cylinder type regular steel structure. Seismic fragility analyses were carried out using twenty-two pairs of earthquake records to obtain the probability of failure for a given earthquake intensity. The validity of the response modification factor used in the seismic design of the model structures was also investigated. Based on the analysis results it was concluded that the response modification factor of 3.0 used in the design of the model structures is acceptable for the ATC-63 methodology. It was also observed that the seismic safety margin for a specific level of earthquake decreases as the vertical irregularity of the structure increases.

Keywords ATC-63 · Tall buildings · Seismic performance factors · Fragility analysis

1 Introduction

Recently the geometric complexity and irregularity of building structures have been rapidly increasing, which significantly affects the seismic performance of the structures. Al-Ali and Krawinkler (1998) investigated the seismic behavior of building structures with vertical irregularities, and found that the seismic response of building structures is more sensitive to stiffness and strength irregularities than to mass irregularities. Soni and Mistry (2006) carried out review of studies on the seismic behavior of vertically irregular structures along with their findings. Scott et al. (2007) explored the structural challenges that are created by buildings with unique geometries or articulated forms, and discussed some of economic design and construction techniques. Sarkar et al. (2010) proposed a new method of quantifying irregularity in building frames with vertical geometric irregularity accounting for dynamic characteristics, and provided a modified empirical formula for estimating fundamental period. Vollers (2008) proposed a morphological scheme which enables data to be retrieved on sustainable performance of building shapes. He categorized the geometry of high-rise buildings into *Extruders, Rotors, Twisters, Tordos, Transformers*, and *Free Shapers* depending on their form-generation method. Kim and Kong (2013) investigated the progressive collapse-resisting capacities of rotor-type diagrid structural system buildings based on arbitrary column removal scenario, and found that the rotor-type diagrid structures showed sufficient progressive collapse-resisting capacity regardless of the differences in shapes as long as they were designed to meet the current design code. Kim and Kwon (2014) investigated the progressive collapse and seismic performance of twisted diagrid buildings. Recently Gerasimidis et al. (2016) proposed a simple approach for optimizing diagonals of steel diagrid tall buildings and discussed on robustness of tall building structures.

The current seismic design codes, however, do not distinguish seismic response factor depending on vertical geometry of structures. The seismic response factors, especially the response modification factor, are important in the evaluation of design seismic load of structures. In the design of tall buildings the response modification factor significantly affects the overall cost of construction and safety. In this study the seismic performance of the Rotor-type or axi-symmetric tall building structures was evaluated by nonlinear static and dynamic analyses. The validity of the seismic performance factor used for seismic design was

✉ Jinkoo Kim
jkim12@skku.edu

[1] Department of Civil and Architectural Engineering, Sungkyunkwan University, Suwon, Korea

Published online: 30 April 2018

also investigated following the procedure recommended in the ATC-63 (2009) report. For analysis models, thirty-three-story convex, concave, and gourd-type axi-symmetric buildings were designed to have similar floor areas using diagrid structure system, and their performances are compared with that of a regular moment frame building. Seismic fragility analyses were carried out using twenty-two pairs of earthquake records to compare the probability of failure of model structures for a given earthquake intensity. The effect of variation in the overall shape of axi-symmetric tall buildings on the seismic performance was also evaluated.

2 Seismic Performance Evaluation Procedure of ATC-63

The ATC-63 recommended a methodology for quantifying building system performance and response parameters for use in seismic design. The methodology achieves the primary life safety performance objective by requiring an acceptably low probability of collapse of the seismic-force resisting system when subjected to maximum considered earthquake (MCE) ground motions. The methodology consists of a framework for establishing seismic performance factors (SPFs) that involves development of detailed system design information and probabilistic assessment of collapse risk. It utilizes nonlinear analysis techniques, and explicitly considers uncertainties in ground motion, modeling, design, and test data. The technical approach is a combination of traditional code concepts, advanced nonlinear dynamic analyses, and risk-based assessment techniques.

Figure 1 defines seismic performance factors in terms of the global inelastic response of the seismic-force-resisting system subjected to MCE ground motions. In this figure, the horizontal axis is lateral displacement and the vertical axis is the lateral force at the base of the system (i.e., base shear). The term, V_E, represents the force level developed in the elastic seismic-force-resisting system. The term, V_{max}, represents the maximum strength of the fully-yielded system, and the term, V, is the seismic base shear required for design. The R factor is the ratio of the force level that would be developed in the elastic system for design earthquake ground motions to the base shear prescribed for design, and the Ω_O factor is the ratio of the maximum strength of the fully-yielded system to the design base shear. The term, δ_E/R, represents roof drift of the seismic-force resisting system corresponding to design base shear, V, and the term, δ, represents the assumed roof drift of the yielded system corresponding to design earthquake ground motions. As illustrated in the figure, the displacement amplification factor C_d is some fraction of the R.

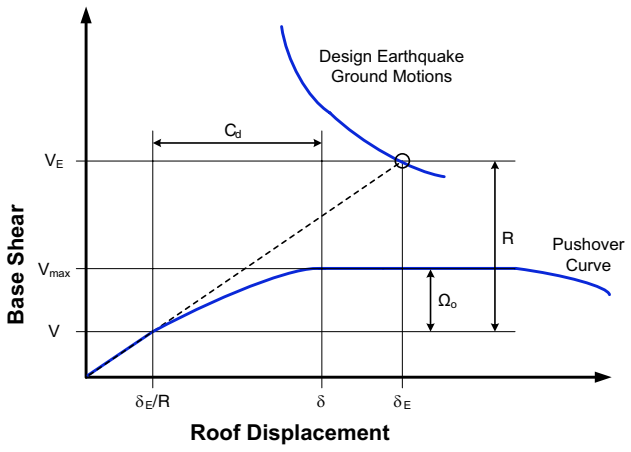

Fig. 1 Definition of seismic performance factors in the *NEHRP Recommended Provisions*

In the ATC-63 collapse assessment is performed using nonlinear static (pushover) and nonlinear dynamic (response history) analysis procedures. Nonlinear static analyses are used to help validate the behavior of nonlinear models and to provide statistical data on system overstrength and ductility capacity. Nonlinear dynamic analyses are used to assess median collapse capacities, and collapse margin ratios. Nonlinear response is evaluated for a set of pre-defined ground motions which include twenty-two ground motion record pairs from sites located greater than or equal to 10 km from fault rupture, referred to as the "Far-Field" record set. Table 1 shows the characteristics of the earthquake records used in the analysis. The ground motions are scaled (or "anchored") to a specific ground motion intensity such that the median spectral acceleration of the record set matches spectral acceleration at the fundamental period of the structure being analyzed. This scaling process parallels the ground motion scaling requirements of ASCE 7-10 (2010).

Nonlinear incremental dynamic analyses are conducted to establish the median collapse capacity and collapse margin ratio (*CMR*) for each of the analysis models. The ratio between the median collapse intensity, $\widehat{S_{CT}}$, and the MCE intensity, S_{MT}, is defined as the collapse margin ratio (*CMR*), which is the primary parameter used to characterize the collapse safety of the structure.

$$\mathrm{CMR} = \frac{\hat{\mathrm{S}}_{\mathrm{CT}}}{\mathrm{S}_{\mathrm{MT}}} = \frac{\mathrm{SD}_{\mathrm{CT}}}{\mathrm{SD}_{\mathrm{MT}}} \tag{1}$$

Determination of the collapse margin ratio for each index archetype model is expected to require approximately 5 analyses of varying intensity for each component of the 22 pairs of earthquake ground motion records. Ground motion intensity, *ST*, is defined based on the median spectral intensity of the Far-Field record set, measured at the fundamental period of the structure. The procedure for conducting nonlinear response history analyses is based on the concept of

Table 1 "Far-field" ground motions used in the ATC-63

Nos.	Record seq. no.	Name	Component 1	Component 2	PGA_{MAX} (g)
1	953	Northridge	NORTHR/MUL009	NORTHR/MUL279	0.52
2	960	Northridge	NORTHR/LOS000	NORTHR/LOS270	0.48
3	1602	Duzce, Turkey	DUZCE/BOL000	DUZCE/BOL090	0.82
4	1787	Hector Mine	HECTOR/HEC000	HECTOR/HEC090	0.34
5	169	Imperial Valley	IMPVALL/H-DLT262	IMPVALL/H-DLT352	0.35
6	174	Imperial Valley	IMPVALL/H-E11140	IMPVALL/H-E11230	0.38
7	1111	Kobe, Japan	KOBE/MIS000	KOBE/MIS090	0.51
8	1116	Kobe, Japan	KOBE/SHI000	KOBE/SHI090	0.24
9	1158	Kocaeli, Turkey	KOCAELI/DZC180	KOCAELI/DZC270	0.36
10	1148	Kocaeli, Turkey	KOCAELI/ARC000	KOCAELI/ARC090	0.22
11	900	Landers	LANDERS/YER270	LANDERS/YER360	0.24
12	848	Landers	LANDERS/CLW-LN	LANDERS/CLW-TR	0.42
13	752	Loma Prieta	LOMAP/CAP000	LOMAP/CAP090	0.53
14	767	Loma Prieta	LOMAP/GO3000	LOMAP/GO3090	0.56
15	1633	Manjil, Iran	MANJIL/ABBAR-L	MANJIL/ABBAR-T	0.51
16	721	Superstition Hills	SUPERST/B-ICC000	SUPERST/B-ICC090	0.36
17	725	Superstition Hills	SUPERST/B-POE270	SUPERST/B-POE360	0.45
18	829	Cape Mendocino	CAPEMEND/RIO270	CAPEMEND/RIO360	0.55
19	1244	Chi–Chi, Taiwan	CHICHI/CHY101-E	CHICHI/CHY101-N	0.44
20	1485	Chi–Chi, Taiwan	CHICHI/TCU045-E	CHICHI/TCU045-N	0.51
21	68	San Fernando	SFERN/PEL090	SFERN/PEL180	0.21
22	125	Friuli, Italy	FRIULIA/A-TMZ000	FRIULIA/A-TMZ270	0.35

incremental dynamic analysis (IDA) (Vamvatsikos and Cornell 2002), in which each ground motion is scaled to increasing intensities until the structure reaches a collapse point.

Collapse is judged to occur either directly from dynamic analysis results (as evidenced by dynamic instability or excessive lateral displacements) or indirectly through non-simulated component limit state criteria. Using collapse data obtained from nonlinear dynamic analyses, a collapse fragility can be defined through a cumulative distribution function (CDF), which relates the ground motion intensity to the probability of collapse (Ibarra et al. 2002). The lognormal distribution is defined by two parameters, which are the median collapse intensity, $\widehat{S_{CT}}$, and the standard deviation of the natural logarithm, β. The median collapse capacity corresponds to a 50% probability of collapse. The slope of the lognormal distribution is measured by β, and reflects the variability (uncertainty) in results. While the IDA concept is useful to illustrate the collapse assessment procedure, the ATC-63 methodology only requires identification of the median collapse point, $\widehat{S_{CT}}$, which can be calculated with fewer nonlinear analyses than would otherwise be required to calculate the full IDA curve. $\widehat{S_{CT}}$ can be obtained by scaling all the records in the Far-Field record set to the MCE intensity, S_{MT}, and then by increasing intensity until one-half of the scaled ground motion records cause collapse. The lowest intensity at which one-half of the records cause collapse is the median collapse intensity, $\widehat{S_{CT}}$. As a result, nonlinear response history analyses are computationally much less involved than the IDA approach. The MCE intensity is obtained from the response spectrum of MCE ground motions at the fundamental period, T.

Baker and Cornell (2006) have shown that rare ground motions corresponding to the MCE have a distinctive spectral shape that differs from the shape of the design spectrum. To account for the effect of spectral shape in determination of the collapse margin ratio, the spectral shape factors, *SSF*, which depend on fundamental period, T, and ductility capacity, μ_C, are used to adjust collapse margin ratios. Table 2 shows the values of spectral shape factor, *SSF*, presented in ATC-63 for various levels of building deformation capacity and various building periods. The adjusted collapse margin ratio (ACMR) is obtained by multiplying tabulated *SSF* values with the collapse margin ratio that was predicted using the Far-Field record set.

Acceptable values of adjusted collapse margin ratio are based on total system collapse uncertainty, β_{TOT}, and established values of acceptable probabilities of collapse. They are based on the assumption that the distribution of collapse level spectral intensities is lognormal, with a median value, $\widehat{S_{CT}}$, and a lognormal standard deviation equal to the total system collapse uncertainty, β_{TOT}.

Table 2 Spectral shape factor (SSF) for structures designed for S_{DS} B, S_{DS} C or S_{DS} D_{min} presented in the ATC-63

T (s)	Period-based ductility, μ_T							
	1.0	1.1	1.5	2	3	4	6	≥8
:	:	:	:	:	:	:	:	:
0.9	1.00	1.03	1.07	1.09	1.13	1.15	1.19	1.22
1.0	1.00	1.04	1.08	1.10	1.14	1.17	1.21	1.25
1.1	1.00	1.04	1.08	1.11	1.15	1.18	1.23	1.27
:	:	:	:	:	:	:	:	:

Table 3 Acceptable values of adjusted collapse margin ratio presented in the ATC-63

Total system collapse uncertainty	Collapse probability				
	5%	10% ($ACMR_{10\%}$)	15%	20% ($ACMR_{20\%}$)	25%
:	:	:	:	:	:
0.650	2.91	2.30	1.96	1.73	1.55
0.675	3.04	2.38	2.01	1.76	1.58
0.700	3.16	2.45	2.07	1.80	1.60
:	:	:	:	:	:

$$\beta_{TOT} = \sqrt{\beta_{RTR}^2 + \beta_{DR}^2 + \beta_{TD}^2 + \beta_{MDL}^2} \quad (2)$$

The total system collapse uncertainty is a function of record-to-record (RTR) uncertainty, design requirements related (DR) uncertainty, test data-related (TD) uncertainty, and modeling (MDL) uncertainty. Quality ratings for design requirements, test data, and nonlinear modeling are translated into quantitative values of uncertainty based on the following scale: (A) Superior, $\beta = 0.20$; (B) Good, $\beta = 0.30$; (C) Fair, $\beta = 0.45$; and (D) Poor, $\beta = 0.65$. Values of total system collapse uncertainty, β_{TOT}, are provided in Table 7-2 of the ATC-63. Table 7-3 of the ATC-63 and Table 3 of this paper provide acceptable values of adjusted collapse margin ratio, *ACMR*10% and *ACMR*20%, based on total system collapse uncertainty and values of acceptable collapse probability, taken as 10 and 20%, respectively.

3 Design and Analysis Modeling of Model Structures

The analysis model structures are 33-story axi-symmetric structures with the cylindrical, convex, concave, and the gourd shapes as shown in Fig. 2. The diagrid system was applied to structural design of the model structures, which has the advantage of being easily adapted to the structure with vertical irregularity. Kim and Lee (2012) compared the seismic performance of thirty-six story diagrid and moment frame buildings, and found that the diagrid structure showed higher overstrength with smaller ductility compared with the moment resisting tubular structure. To compare the seismic performances on equal basis, the model structures were designed to have similar total floor area. Figure 3 depicts the structural plan shape of the cylinder type structure depicting the location of the vertical members. The floor beams were pin connected to the columns and the diagrid members. The perimeter beams were designed with H-shaped rolled sections with ultimate strength of 400 N/mm^2, and the core columns were designed with box shaped steel with ultimate strength of 490 N/mm^2. The diagrid members were designed with circular hollow steel sections with ultimate strength of 490 N/mm^2. The floor slabs were considered as rigid diaphragm. The model structures were designed with the dead and live loads of 6 and 2.5 kN/m^2, respectively, and wind load with basic wind speed of 30 m/s. The seismic load was evaluated based on the spectral acceleration coefficients of $S_{DS} = 0.43$ and $S_{D1} = 0.23$ with the response modification factor of 3.0 in the ASCE 7-10 (2010) format. The structural design was carried out using the structural analysis/design program code MIDAS (2007) based on the AISC LRFD Specifications (2000). Tables 4 and 5 show the member sizes of exterior diagrid bracing and perimeter girders, respectively, at selected stories. Figure 4 depicts the distribution of story mass and story stiffness of model structures along the height. Table 6 shows the total floor areas and fundamental periods of the model structures. As mentioned before the model structures were designed to have similar total floor areas. The natural period of the gourd type structure is the longest and that of the cylinder type structure is the shortest. It also can be observed that the natural period is larger in the model structures with their vertical center of mass located at higher levels. The convex type structures with relatively high aspect ratio (height to width ratio) have larger period than concave type structures with small aspect ratio. Table 7 shows the design base shears and steel tonnages of the model structures. The numbers in the parenthesis represent the ratio of the design base shear and steel tonnage of that structure with respect to those of the cylinder type structure. It can be observed that the cylinder type structure with no irregularity (CYL) and the structure with smallest aspect ratio (CV-L) were designed with the smallest design base shear. It can be observed that the smallest amount of structural steel was

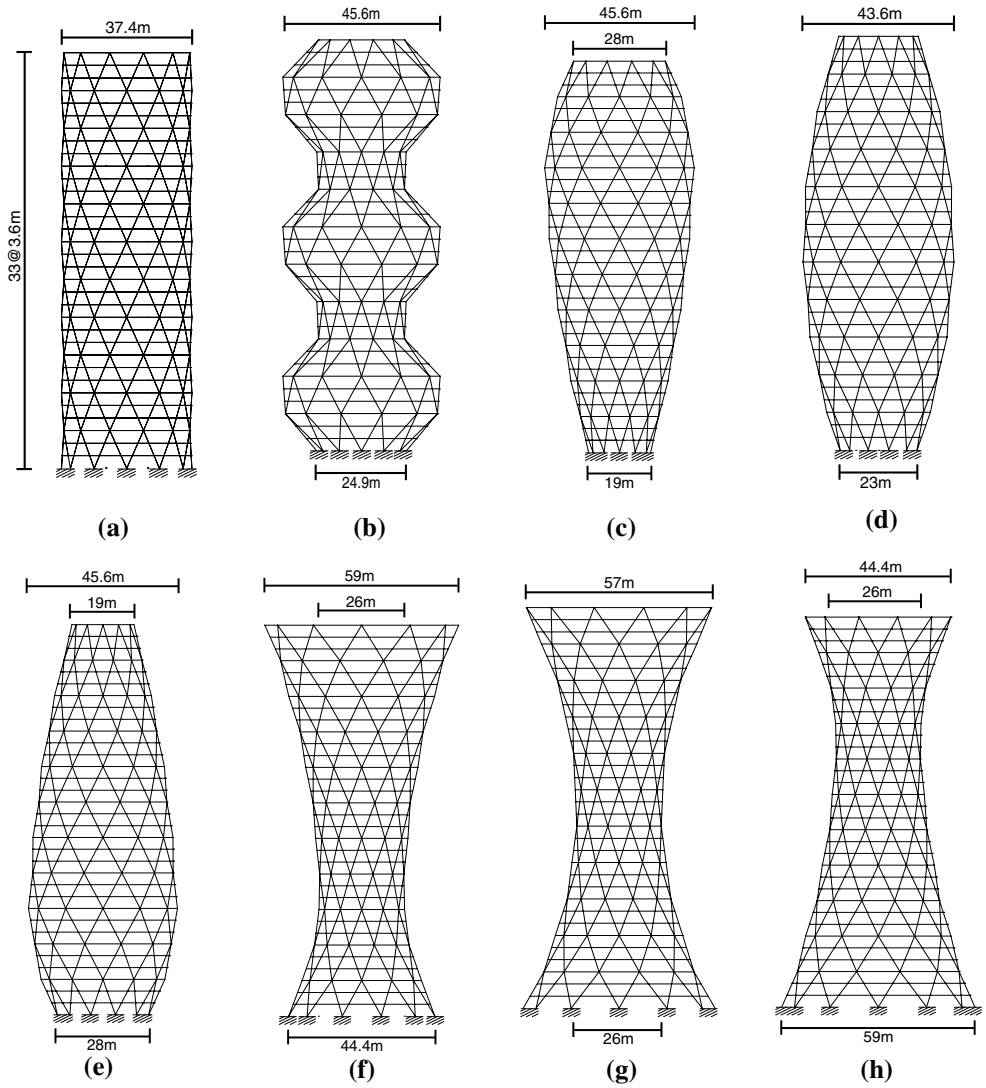

Fig. 2 Elevation of 33-story analysis model structures. **a** CYL, **b** GOU, **c** CV_H, **d** CV_M, **e** CV_L, **f** CC_H, **g** CC_M, **h** CC_L

used in the design of cylinder type structure with no vertical irregularity, and the largest steel was used in the gourd type structure with largest vertical irregularity.

For nonlinear analysis of bending members the skeleton curve provided in the FEMA-356 (2000) and shown in Fig. 5a was used. The parameters *a, b*, and *c* vary depending on the width-thickness ratio of the structural members, and were determined based on the guidelines provided in the Tables 5-6 and 5-7 of the FEMA-356. The post-yield stiffness of 3% was generally used for modeling of bending members. Figure 5a also shows the deformation levels corresponding to the immediate occupancy (IO), life safety (LS), and collapse prevention (CP) performance points as specified in the FEMA 356. For nonlinear analysis of bracing members, the generalized load-deformation curves recommended in the FEMA-274 (1997) and shown in Fig. 5b were used.

4 Seismic Performance Evaluation of Model Structures

4.1 Nonlinear Static Analysis Results

The pushover analyses of the model structures were conducted using the following lateral load pattern which includes the first three vibration modes (Freeman et al. 1998; Requena and Ayala 2000):

$$F_i = \sqrt{\sum_{i=1}^{N} \left\{ \left(\frac{\sum_{k=1}^{N} m_k \varphi_{kj}}{\sum_{k=1}^{N} m_k \varphi_{kj}^2} \right) \varphi_{ij} S_{aj} m_i \right\}^2} \tag{3}$$

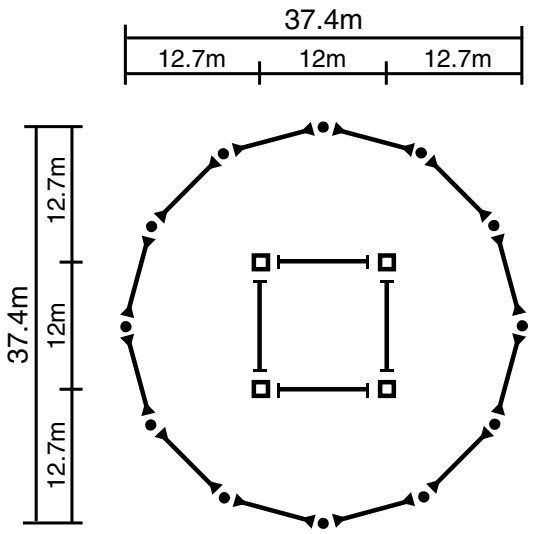

Fig. 3 Floor plan of the cylinder type case study buildings

Table 4 Member size of exterior diagrid structure at selected stories

	1-story	11-story	22-story	33-story
CYL	P 609.6×19	P 508.0×22	P 406.4×16	P 190.7×5
GOU	P 1016.0×22	P 609.6×19	P 508.0×12	P 165.2×7
CV_H	P 812.8×22	P 609.6×22	P 457.2×16	P 165.2×5
CV_M	P 812.8×22	P 609.6×22	P 406.4×12	P 190.7×6
CV_L	P 711.2×22	P 558.8×16	P 355.6×9	P 190.7×4.5
CC_H	P 711.2×19	P 609.6×19	P 609.6×16	P 355.6×8
CC_M	P 609.6×22	P 609.6×19	P 508.0×16	P 318.5×8
CC_L	P 609.6×22	P 508.0×16	P 508.0×16	P 190.7×7

where F_i and m_i are the story force and story mass of the ith story, respectively; N is the number of story; $\boldsymbol{\Phi}_{ij}$ is the mode shape coefficient of the ith story in the jth mode; and S_{aj} is the spectral acceleration of the jth mode. The vertical distribution patterns of the lateral load for analysis model structures are shown in Fig. 6. Requena and Ayala (2000) showed that the lateral displacement and the plastic hinge distribution of a structure obtained using the above equation corresponded with the nonlinear dynamic analysis results better than those obtained by the lateral load distribution proportional to the first mode. Pushover analyses were carried out using the nonlinear analysis code Perform-3D (2006) to obtain the load–displacement relationships and the plastic hinge formation of the model structures. Figure 7 shows the pushover curves of the model structures. The vertical axis represents the base shear normalized with the design base shear, and the horizontal axis represents the top-story displacement. It was observed that the strength dropped sharply right after the initial failure of a few members. Except for the Gourd type structure, the lateral load-resisting capacities of the model structures decreased rapidly before the maximum inter-story drifts reached 2% of the story height. The stiffness and strength are the largest in the cylinder-type structure and are the smallest in the gourd type structure. The gourd type structure has the longest natural period, and as the model structures were designed to have similar total floor area, they have similar mass. This implies that the stiffness of the GOU model is significantly smaller than those of the other structures. The overstrength is larger in the structures with low center of mass such as CV_L and CC_L. The opposite is true in the structures with their center of mass at or higher than the mid-height of the structure. Figure 8 depicts the locations of plastic hinges or buckled members in the model structures when the lateral load was applied from the left-hand-side. It was observed that plastic hinges first form at the lower stories where story shear is large, and are spread to higher stories as the applied load increases. The amount of inelastic deformation of the members can be identified by the plastic hinge definition denoted in Fig. 8 referring to the force–deformation relationships for structural members shown in Fig. 5. In the cylinder-type structures collapse was initiated by buckling of the diagrids located in the lower right-hand-side. It also can be observed that in the convex-type structures buckled or yielded members are concentrated in the lower few stories, whereas in the concave-type structures such members are distributed more widely in the right hand side of the structures. In the gourd type structure inelastic deformation was concentrated in the concave parts of the structure. Based on the plastic

Table 5 Member size of perimeter beams at selected stories

	1-story	11-story	22-story	33-story
CYL	H 404×201×9/15	H 404×201×9/15	H 404×201×9/15	H 606×201×12/20
GOU	H 300×150×6.5/9	H 300×150×6.5/9	H 300×150×6.5/9	H 350×175×7/11
CV_H	H 386×299×9/14	H 386×299×9/14	H 600×200×11/17	H 582×300×12/17
CV_M	H 434×299×10/15	H 434×299×10/15	H 434×299×10/15	H 588×300×12/20
CV_L	H 386×299×9/14	H 482×300×11/15	H 386×299×9/14	H 588×300×12/20
CC_H	H 708×302×15/28	H 404×201×9/15	H 404×201×9/15	H 912×302×18/34
CC_M	H 692×300×13/20	H 400×200×8/13	H 400×200×8/13	H 900×300×16/28
CC_L	H 588×300×12/20	H 588×300×12/20	H 396×199×7/11	H 792×300×14/22

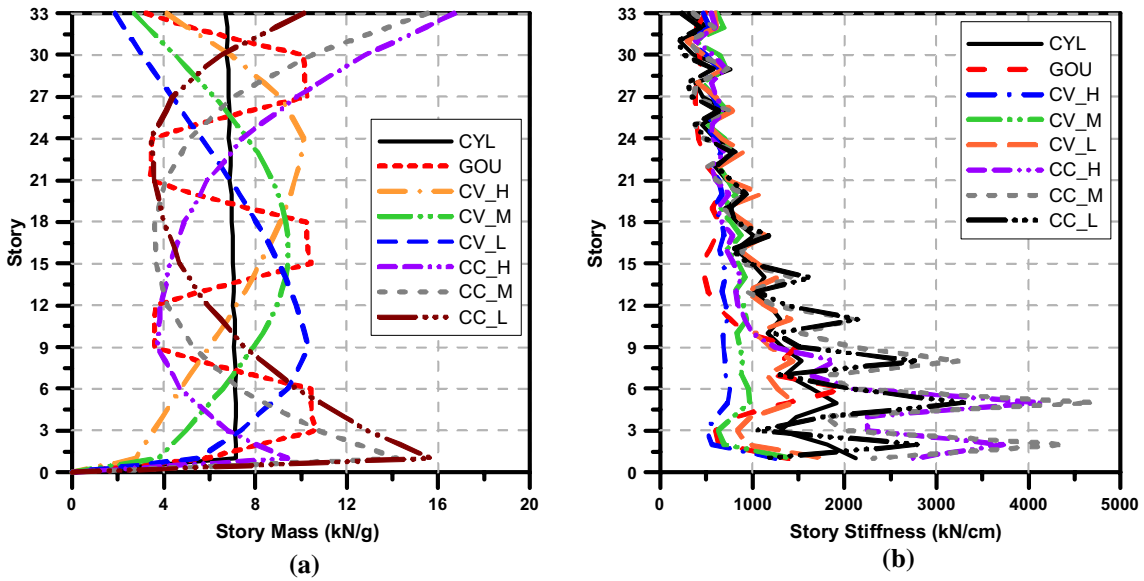

Fig. 4 Story mass and story stiffness of analysis model structures. **a** Story mass and **b** story stiffness

Table 6 Total floor area and fundamental period of analysis model structures

Type	Total floor area (m^2)	Fundamental period (s)
CYL	34,981	3.26
GOU	35,120	6.77
CV-H	34,965	5.29
CV-M	34,839	4.19
CV-L	35,325	3.44
CC-H	34,284	4.57
CC-M	34,692	3.92
CC-L	35,308	3.33

Table 7 Design base shear and steel tonnage of the model structures

Type	Design base shear (kN)	Weight of perimeter structure (tonf)
CYL	6880.27 (1.00)	1660 (1.00)
GOU	7026.69 (1.02)	2095 (1.26)
CV-H	7009.24 (1.02)	1897 (1.14)
CV-M	10,164.27 (1.48)	1850 (1.11)
CV-L	6878.12 (1.00)	1670 (1.01)
CC-H	10,390.13 (1.51)	2102 (1.27)
CC-M	10,145.01 (1.47)	1910 (1.15)
CC-L	7098.09 (1.03)	1721 (1.04)

hinge distribution patterns of the model structures, it can be observed that a sudden change in the vertical shape of the model structure leads to an abrupt change in the angles of the diagonals, which likely causes the concentrated damage in the structures. This, however, may be prevented by optimum design of diagrid configurations as tried by Gerasimidis et al. (2016).

4.2 Validity of the Response Modification Factor

In this section the collapse potential and the validity of the seismic performance factors used in the design of the model structures were investigated based on the ATC 63 procedure. The 44 ground motions presented in Table 1 were collectively scaled in such a way that the median spectral acceleration of the record set matches the MCE design spectral acceleration at the fundamental period of the model structures. Plots of the response spectra for the record set, and an illustration of intensity anchoring to the MCE design spectrum corresponding to the fundamental natural period of the cylinder-type model structure, are shown in Fig. 9. Collapse was judged to occur from dynamic instability at which excessive displacement occurred without increase in spectral acceleration. Incremental dynamic analyses were carried out increasing the intensity of the records by 0.02 g until dynamic instability occurred for 22 earthquake records. It was observed that plastic hinges formed randomly throughout the height due to the participation of the higher modes of vibration. The median collapse intensity or the spectral acceleration ($\hat{S}_{CT}$) at which dynamic instability of each model structure was initiated by the 22nd earthquake record was determined from the IDA curves. The state of dynamic instability was defined as the point at which the stiffness of the structure decreased to 20% of the initial stiffness based

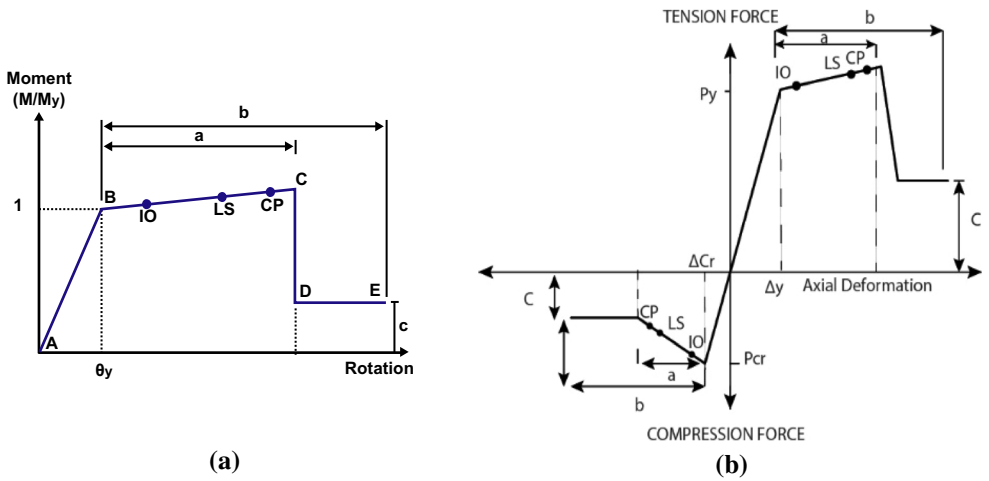

Fig. 5 Nonlinear force–deformation relationships for structural members. **a** Flexural members, **b** braces

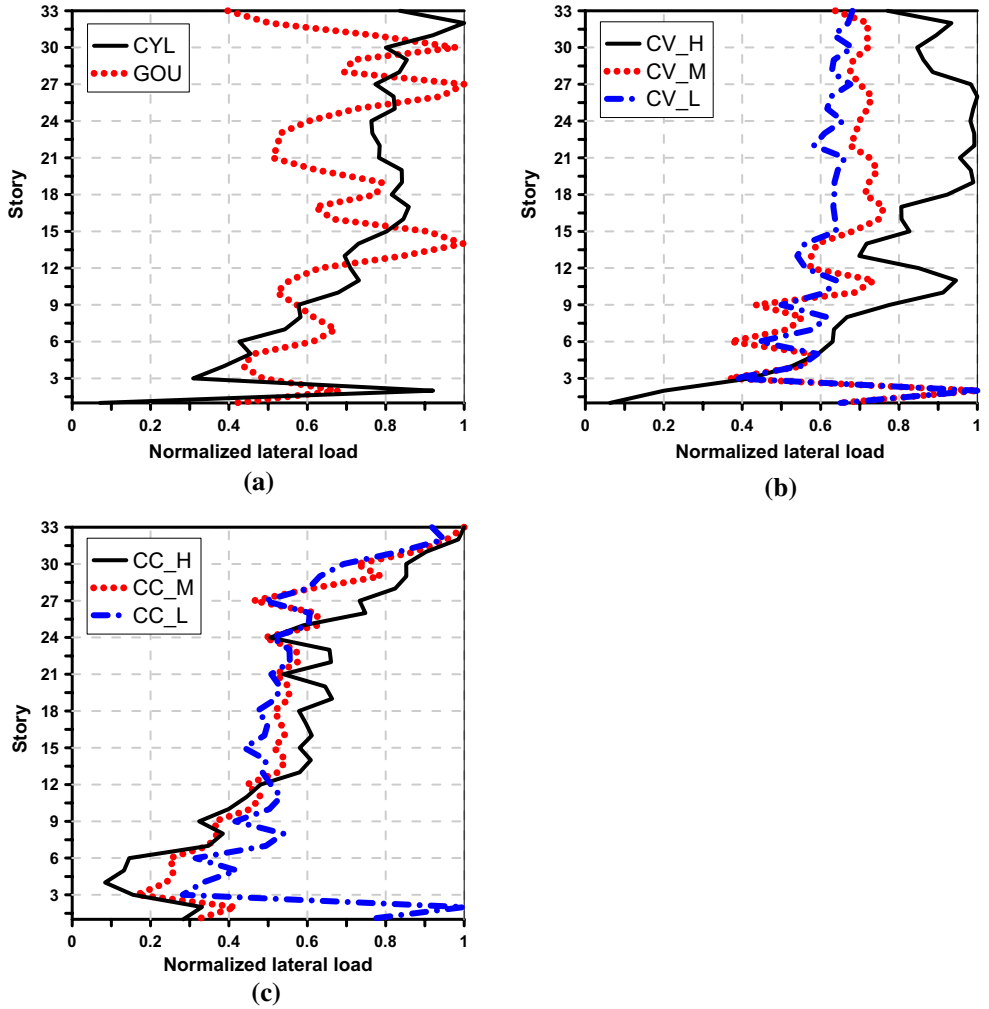

Fig. 6 Lateral load patterns used for pushover analysis of model structures. **a** Cylinder and gourd type, **b** convex type and **c** concave type

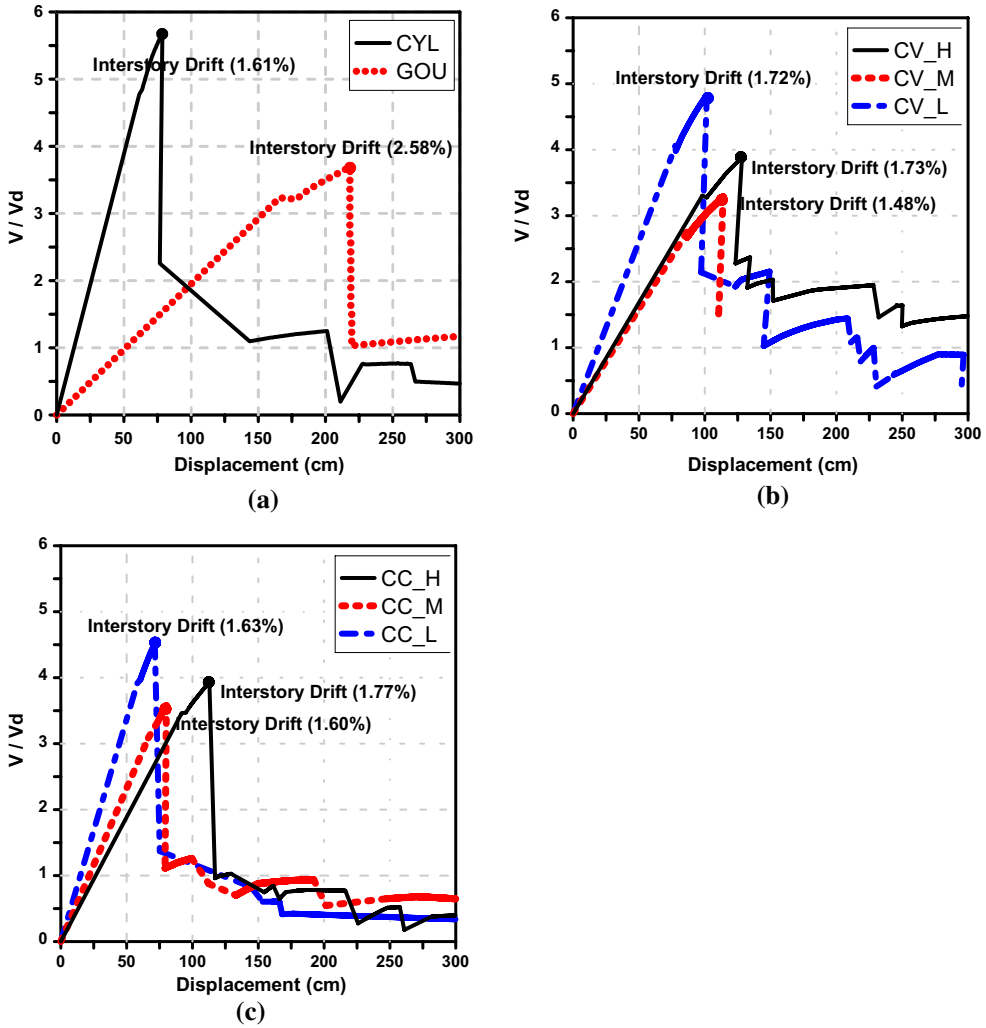

Fig. 7 Nonlinear static analysis results of various axi-symmetric structures. **a** Cylinder and gourd, **b** convex, **c** concave

on Vamvatsikos and Cornell (2002). Table 8 summarized such information as the MCE spectral acceleration, S_{MT}, the median collapse capacity, $\widehat{S_{CT}}$, and the collapse margin ratio (*CMR*) of the model structures obtained from incremental dynamic analysis results. It can be observed that the cylinder-type structure with no irregularity has the largest values for the MCE spectral acceleration, the median collapse capacity, and the margin for collapse followed by the concave-type structure with low center of mass (CV_L) in which large part of mass is concentrated in the lower stories. The spectral acceleration at collapse and the CMR of the gourd-type structure are the smallest followed by the concave structure with high center of mass (model CC_H). As the natural period increases and as the location of the center of mass increases, the MCE spectral acceleration, the median capacity, and the CMR tend to decrease. The collapse margins for concave-type structures turned out to be generally higher than those of the convex-type structures.

Table 9 shows the period based ductility factors and the spectral shape factors (SSF) of the model structures obtained from linear interpolation of the SSF presented in Table 7-1 of the ATC-63. Also shown are the adjusted collapse margin ratios (ACMR) of the model structures obtained by multiplying the SSF with the CMR. Even though the gourd-type model has the smallest CMR, the adjusted value, ACMR, is the smallest in the CC_H structure. Table 7-3 of ATC-63 provides acceptable values of adjusted collapse margin ratio, *ACMR*10% and *ACMR*20%, based on total system collapse uncertainty and values of acceptable collapse probability, taken as 10 and 20%, respectively. Lower values of acceptable collapse probability and higher levels of collapse uncertainty result in higher required values of adjusted collapse margin ratio. Acceptable performance is achieved when individual values of adjusted collapse margin ratio for each structure exceeds *ACMR*20%. As diagrid structure systems

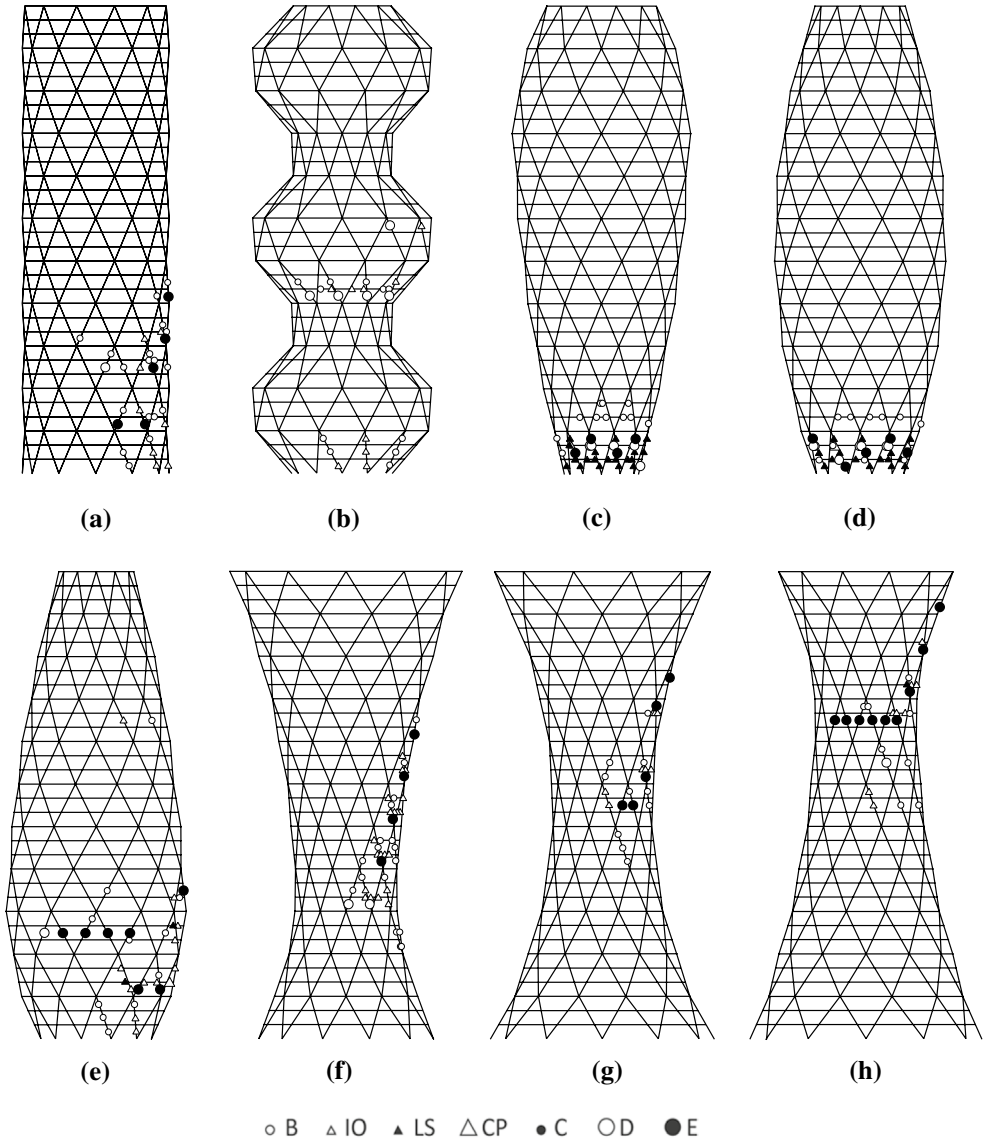

Fig. 8 Plastic hinge formation in the various axi-symmetric structures. **a** CYL**, b** GOU**, c** CV_H, **d** CV_M, **e** CV_L, **f** CC_H, **g** CC_M, **h** CC_L

are relatively newly developed and there are no seismic performance factors recommended yet in the design codes, the quality rating for the design requirements was considered to be (C) Fair ($\beta_{DR} = 0.35$). The rating for the test data-related uncertainty was assumed to be (B) Good ($\beta_{TD} = 0.2$), and the modeling uncertainty was also assumed to be (B) Good ($\beta_{MDL} = 0.2$). The uncertainty due to record-to-record variability is recommended to be $\beta_{RTR} = 0.40$ in the ATC-63. The total system collapse uncertainty for the analysis model structures was calculated to be 0.602 using Eq. 2. From Table 7-3 of the ATC-63, the collapse probability of the model structures are obtained as ACRM 20% = 1.66, which is smaller than the ACMR of the model structures. Based on this result, it can be concluded that the seismic performance factors, especially the response modification factor, are appropriate for the seismic design of the analysis model structures with axi-symmetric diagrid system.

5 Fragility Analysis

Fragility curves show the probability of a system reaching a limit state as a function of some measure of seismic intensity. In this study pseudo spectral acceleration was used as the seismic intensity measure. The state of dynamic instability was considered as the limit state for failure. The seismic fragility is described by the conditional probability that the structural capacity, *C*, fails to resist the structural demand, *D*, given the seismic intensity hazard, *SI*, and is modeled

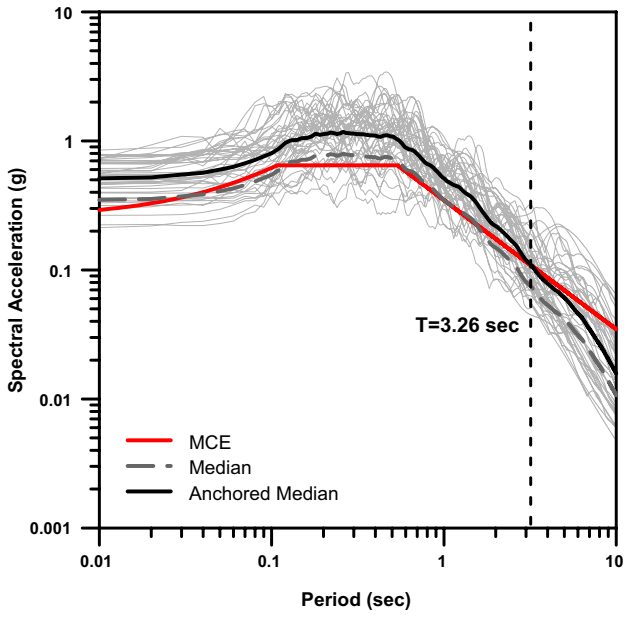

Fig. 9 Response spectra for the record set and intensity anchoring to the MCE design spectrum corresponding to the fundamental natural period of the cylinder-type model structure

Table 8 Collapse margin ratios of the model structures

Type	S_{MT}	$\widehat{S_{CT}}$	CMR
CYL	0.107	0.240	2.243
GOU	0.051	0.085	1.667
CV-H	0.066	0.130	1.970
CV-M	0.083	0.182	2.193
CV-L	0.101	0.225	2.228
CC-H	0.076	0.127	1.671
CC-M	0.089	0.180	2.022
CC-L	0.104	0.218	2.096

Table 9 Adjusted collapse margin ratios of the model structures

Type	μ_T	SSF	ACMR
CYL	1.249	1.072	2.404
GOU	1.394	1.094	1.824
CV-H	1.369	1.090	2.147
CV-M	1.323	1.083	2.375
CV-L	1.311	1.082	2.411
CC-H	1.271	1.076	1.798
CC-M	1.227	1.069	2.161
CC-L	1.253	1.073	2.249

by a lognormal cumulative distribution function as follows (Celik and Ellingwood 2009):

$$P[C < D|SI = x] = 1 - \Phi\left[\frac{\ln(\hat{C}/\hat{D})}{\sqrt{\beta_{D|SI}^2 + \beta_C^2 + \beta_M^2}}\right] \quad (4)$$

where $\Phi[\cdot]$ = Standard normal probability integral, $\hat{C}$ = median structural capacity, associated with the limit state, $\hat{D}$ = median structural demand, $\beta_{D|SI}$ = uncertainty in D, β_C = uncertainty in C, β_M = modeling uncertainty. Figure 10 depicts the fragility curves of the analysis model structures obtained from IDA results of the 22 pairs of ground motions. The total system collapse uncertainty, β_{TOT}, which was used to obtain the acceptable values of adjusted collapse margin ratio in the previous section, was used for the uncertainty in the normal probability integral function Φ. It was observed that the collapse probabilities of the model structures CC_H, CC_M, and CV_H for MCE level earthquakes exceed 10%, while those of the other structures are below that value. The margin for collapse, which was defined as the difference between the MCE ground motion and the spectral accelerations corresponding to the 50% probability of collapse, was also indicated on the figures. It can be observed that the collapse margin for the cylinder-type structure is the largest and that of the gourd-type structure is the smallest. The collapse margins for the structures with low center of mass turned out to be larger than those of the structures with high center of mass. The collapse margins for the convex structures are slightly larger than those of the concave structures.

6 Conclusions

In this study the seismic performances of axi-symmetric diagrid building structures with various vertical irregularities were evaluated based on the procedure recommended in the ATC-63. Seismic fragility analyses were carried out using twenty-two pairs of earthquake records to compare the probability of failure for a given earthquake intensity. The thirty-three story analysis model structures with different elevations were designed to have similar total floor areas, the aspect ratios of the model structures range from 2.0 in the case of the concave structure with low center of mass and to 6.2 in the case of convex structure with high center of mass.

According to the incremental dynamic analysis and fragility analysis of the model structures, the adjusted collapse margin ratios of the model structures turned out to be higher than the acceptable values specified in the ATC-63. The collapse margin ratio of the cylinder-type structure with no vertical irregularity turned out to be larger than those of the other structures with vertical irregularity. The gourd-type structure with longest natural period and highest vertical irregularity showed the smallest collapse margin even though it was designed with the largest steel tonnage. The collapse margins of the structures with low center of mass were generally larger than those of the structures with high center of mass. The collapse margins for the convex structures are slightly larger than those of the concave structures. The structures with high aspect ratios such as the convex

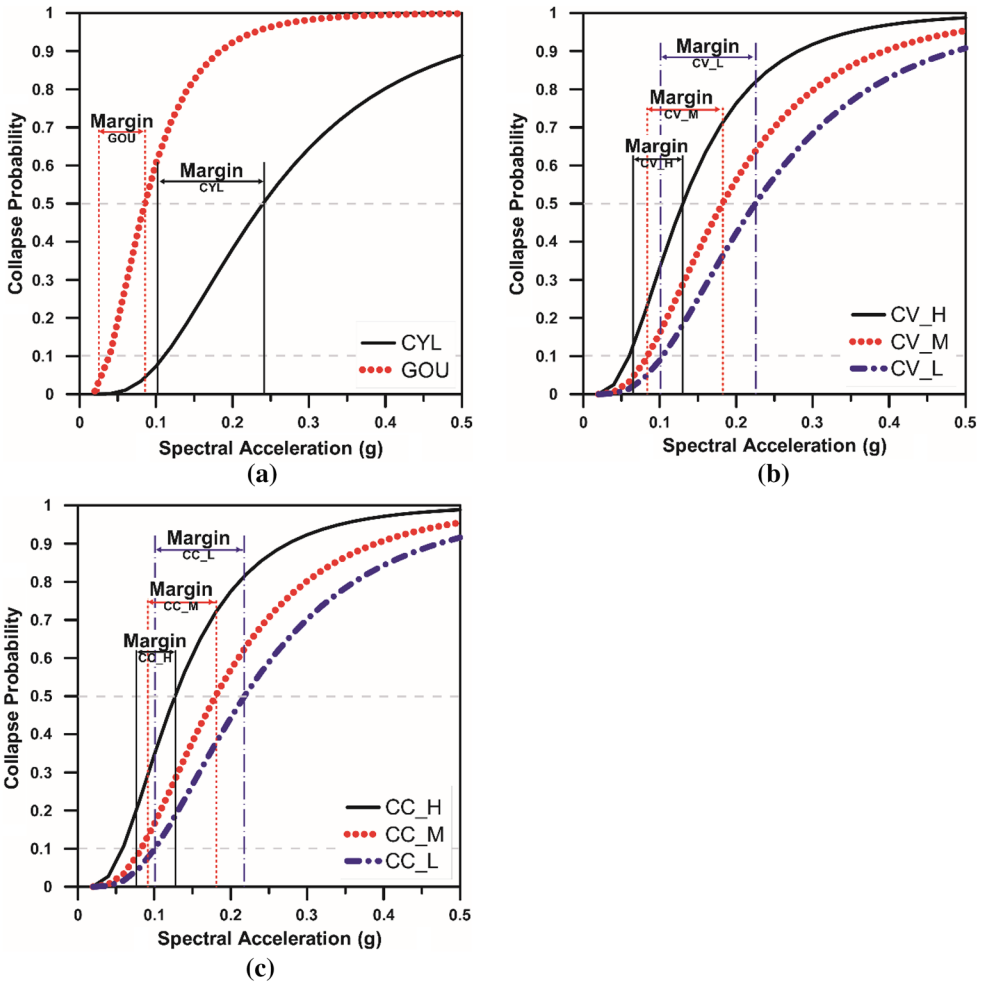

Fig. 10 Fragility curves of the model structures obtained from twenty-two pairs of earthquake records. **a** Cylinder type, **b** convex type and **c** concave type

type with middle or high mass center showed relatively large adjusted collapse margin ratio. The structures with relatively longer natural period such as the gourd type structure and the structures with higher location of mass center showed relatively small adjusted collapse margin ratio. Based on the adjusted collapse margin ratios of the model structures obtained from fragility analyses, it was concluded that the seismic safety decreased as the vertical irregularity of the structure increased, and that the response modification factor of 3.0 used in the design of the model structures was acceptable.

Acknowledgements This research was supported by a Grant (Code 17CTAP-C132889-01) from Technology Advancement Research Program (TARP) funded by Ministry of Land, Infrastructure and Transport of Korean government.

References

AISC. (2000). *Load and resistance factor design specification for structural steel buildings*. Chicago: American Institute of Steel Construction.

Al-Ali, A. K., & Krawinkler, H. (1998). *Effects of vertical irregularities on seismic behavior of building structures*. Report no. 130, Stanford University.

ASCE. (2010). *Minimum design loads for buildings and other structures*. Reston: ASCE Standard ASCE/SEI 7-10, American Society of Civil Engineers.

ATC. (2009). *Quantification of building seismic performance factors*. Redwood City: ATC-63, Applied Technology Council.

Baker, J. W., & Cornell, C. A. (2006). Spectral shape, epsilon and record selection. *Earthquake Engineering and Structural Dynamics, 34*(10), 1193–1217.

Celik, O. C., & Ellingwood, B. R. (2009). Seismic risk assessment of gravity load designed reinforced concrete frames subjected to Mid-America ground motions. *Journal of Structural Engineering, 135*(4), 414–424.

FEMA. (1997). *NEHRP Commentary on the guidelines for the seismic rehabilitation of buildings*. Washington: FEMA-274, Federal Emergency Management Agency.

FEMA. (2000). *Prestandard and commentary for the seismic rehabilitation of buildings*. Washington: FEMA-356, Federal Emergency Management Agency.

Freeman, S., Sasaki, K., & Paret, T. (1998). Multi-mode push-over procedure (MMP). In *Proceedings of 6th national conference on earthquake engineering, EERI, Seattle, Washington.*

Gerasimidis, S., Pantidis, P., Knickle, B., & Moon, K. S. (2016). Diagrid structural system for high-rise buildings: Applications of a simple stiffness-based optimized design. *International Journal of High-Rise Buildings, 5*(4), 319–326.

Ibarra, L., Medina, R., & Krawinkler, H. (2002). Collapse assessment of deteriorating SDOF systems. In *Proceedings of the 12th European conference on earthquake engineering*. London: Elsevier, paper #665. 2002.

Kim, J., & Kong, J. (2013). Progressive collapse behavior of rotor-type diagrid buildings. *The Structural Design of Tall and Special Buildings, 22,* 1199–1214.

Kim, J., & Kwon, K. (2014). Progressive collapse and seismic performance of twisted diagrid buildings. *International Journal of High-Rise Buildings, 3*(3), 223–230.

Kim, J., & Lee, Y. (2012). Seismic performance evaluation of diagrid system buildings. *The Structural Design of Tall and Special Buildings, 21,* 736–749.

MIDAS, G. (2007). *General structure design system for windows*. Bundang-gu: MIDAS Information Technology Co Ltd.

PERFORM-3D. (2006). *Nonlinear analysis and performance assessment for 3D structures-user guide*. Berkeley: Computers and Structures.

Requena, M., & Ayala, G. (2000). Evaluation of a simplified method for the determination of the nonlinear seismic response of RC frames. In *12th world conference on earthquake engineering, Auckland, New Zealand.*

Sarkar, P., Prasad, A. M., & Menon, D. (2010). Vertical geometric irregularity in stepped building frames. *Engineering Structures, 32,* 2175–2182.

Scott, D., Farnsworth, D., Jackson, M., & Clark, M. (2007). The effects of complex geometry on tall towers. *The Structural Design of Tall and Special Buildings, 16,* 441–455.

Soni, D. P., & Mistry, B. B. (2006). Qualitative review of seismic response of vertically irregular building frames. *ISET Journal of Earthquake Technology, Technical Note, 43*(4), 121–132.

Vamvatsikos, D., & Cornell, C. A. (2002). Incremental dynamic analysis. *Earthquake Engineering and Structural Dynamics, 31*(3), 491–514.

Vollers, K. (2008). Morphological scheme of second-generation non-orthogonal high-rises. In *CTBUH 8th world congress.*